Design and characterization of a dual-band miniaturized circular antenna for deep in body biomedical wireless applications

Shuoliang Ding[1] [ID], Stavros Koulouridis[2] [ID] and Lionel Pichon[1] [ID]

[1]Group of Electrical Engineering – Paris, UMR 8507 CNRS, CentraleSupelec, Université Paris-Sud, Sorbonne Université, Gif-sur-Yvette, France and [2]Electrical and Computer Engineering Department, University of Patras, Patras, Greece

CAMBRIDGE
UNIVERSITY PRESS

Abstract

In this paper, a novel miniaturized implantable circular antenna is presented. It supports both wireless information communication and wireless energy transmission at the Medical Device Radiocommunication band (MedRadio 402–405 MHz) and the industrial, scientific, and medical bands (ISM 902.8–928 MHz). The antenna is circular to avoid sharp edges while miniaturization is achieved by adding two circular slots to the patch. The main scenario includes embedding into the muscle layer of a cylindrical three-layer model of a human arm for which several parameters are analyzed (resonance, radiation pattern, and specific absorption rate). Power transmission efficiency and interaction distance limits to ensure connections are also evaluated. Finally, the design is validated by an experimental measurement in an anechoic chamber, and some new improvements are proposed.

Introduction

Recently, with the population's aging acceleration, health care has gained more and more focus in the society. Implantable medical devices (IMDs) have attracted much attention and have been popularly studied thanks to their huge potential to be light, small, and utilized in various pragmatic applications. However, the question of designing an efficient system that supports both power and data transmission for IMDs remains crucial for researchers.

Radiation, as one of the mainly used methods for wireless charging, is more robust to location change and has a smaller size of the reception device compared with the induction and the midfield transmission method. For biomedical uses, several frequency bands are authorized: Medical Device Radiocommunication (MedRadio) service band (401–406 MHz), and the industrial, scientific, and medical (ISM) bands (433.1–434.8, 868–868.6, 902.8–928 MHz, and 2.4–2.5 GHz) [1–3]. Since the team of Chirwa [4] has published a study about the performances of an implanted source in human intestine under different frequencies in 2003, many research teams have carried out successively their own designs or analyses [5–7]. Some designs of antenna possess multiple resonant frequencies but have larger sizes [8]; others are smaller in size but resonate at higher frequency which will certainly lead to higher losses in deeper implantation [9]; moreover, much research is performed in the skin layer, which adds difficulties to medical surgery and is less realistic [10, 11].

In order to address such issues, authors proposed a miniaturized circular antenna in [12]. The antenna has two different resonant frequencies at 403 and 915 MHz which correspond to data and power transmission, respectively. Furthermore, the antenna is designed to be implanted deep into the muscle tissue and not relatively sensitive to the variations of implantation depth and thus robust to changes in the environment. A full wave 3D simulation of the global wireless link showed the validity of the above.

This paper is an extended version of the work presented in [12]. Here, an experimental validation of the design is added, including more details on the experimental process and a comparison between simulations in human and pork tissues. Pork tissue is usually used in validation measurements. Furthermore, the antenna design is improved in order to achieve a good performance during the experiment. The experimental validation of the wireless link with the fabricated proposed antenna is performed in an anechoic chamber. Ground pork meat is used as a biological surrounding environment of the antenna. A comparison between the numerical prediction of the reflection coefficient and the measurement results validates our approach.

In the "Antenna design" section, detailed structure of the antenna is first presented. Numerical results (such as reflection coefficient, impedance, radiation pattern, and specific absorption rate (SAR)) are subsequently analyzed in the "Antenna characteristics" section. Then in the "In-body/off-body interaction" section, the in-body/off-body interaction with
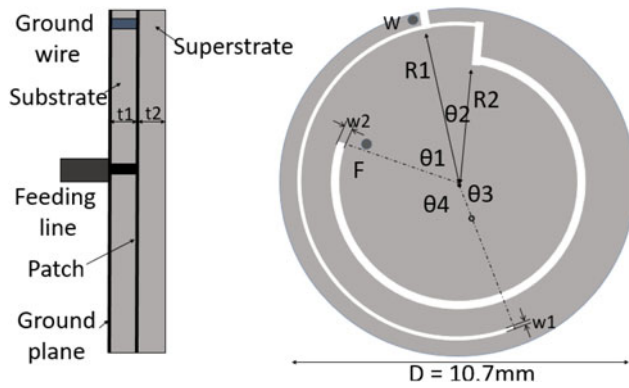
Fig. 1. Geometry of the developed circular antenna.

Table 1. Antenna parameters

Parameter	Value (mm)	Parameter	Value (deg)
R_1	4.9	θ_1	70
R_2	3.76	θ_2	18
w_1	0.15	θ_3	163
w_2	0.32	θ_4	109
t_1	0.64		
t_2	0.64		
D	10.7		

an external dipole is analyzed. Finally, in the "Experimental measurements" section, the measurement scenario and results are presented for a well-defined environment.

Antenna design

A precise parametric model of the antenna is shown in Fig. 1. It is made up of a ground plane, a patch, a substrate between them, a superstrate over the patch, and a coaxial feeding. The substrate and superstrate are made from the same material: Rogers RO 3210 ($\varepsilon_r = 10.2$, $\tan \delta = 0.003$). Both the patch and the ground plane are circular, connected with a ground wire (located at point W, diameter: 0.3 mm) which helps decrease the antenna size. Two circular slots are also cut from the patch in order to have two operating frequencies at 402 and 915 MHz. The impedance of the coaxial cable (located at point F) is standardized to 50 Ω. All the parameters marked in Fig. 1 are presented in Table 1.

The antenna has a circular shape to avoid sharp edges. Table 2 presents the comparison results between the circular Planar Inverted-F Antennas that are designed in previous publications and the antenna designed in this paper, which is smaller, embedded deeper, and resonating at lower frequencies to reduce losses.

The antenna in this paper is analyzed in a more detailed model of the tissue as compared with previous studies. In [7], the antenna is embedded only 3 mm deep which is not as realistic as in this paper because the implantation at this depth is more vulnerable and more difficult to realize. In [9], the study is performed with anatomical tissues and thus is for more specific uses and less useful for other general implantation cases. The implantation depth is 10 mm which is less deep and the antenna is slightly larger compared with the antenna in this paper. In [11] and [13], antennas are implanted into larger skin boxes. It is less realistic since human skins are usually not that thick.
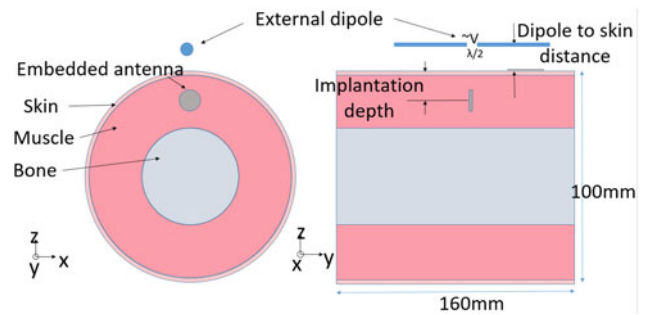

Fig. 2. Geometry of the three-layer arm model.

The antenna in this paper is embedded in the human tissue model shown in Fig. 2. As in [6], a three-layer cylindrical human arm model is used in this paper. The radius of each layer is: bone: 25 mm, muscle: 25–47.5 mm, and skin: 47.5–50 mm. The implantation depth is calculated as the distance between the center of the radiating patch and the external surface of the skin layer. The length of the "arm" is set to the minimum value to ensure proper consideration of a "realistic" case and avoid heavy calculations.

Antenna characteristics

Reflection coefficients

Reflection coefficient is a key factor to characterize the resonant frequency of an antenna. Figures 3(a) and 3(b) characterize the reflection coefficient (S_{11}) of the proposed antenna when implanted into the three-layer arm model at the depth from 10 to 16 mm at 403 and 915 MHz. The dielectric constants of human tissue (relative permittivity ε_r and electrical conductivity σ) at the corresponding frequencies are shown in Table 3. The data in Table 3 are

Table 2. Comparison with previous designs

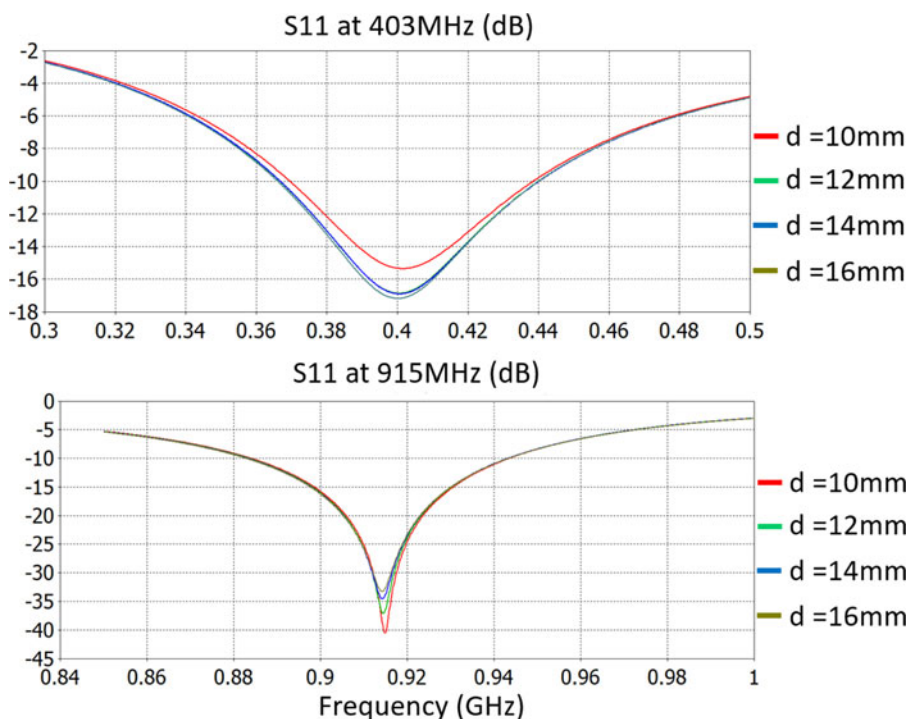| Reference	Antenna radius (mm)	Gain in tissue (dB)	Resonant frequency (GHz)	Examined depth (mm)	Model used
[7]	8.5	−15	2.4	2–3	Muscle + phantom
[9]	6	−33.41	0.4; 0.9	10	Skin cube
[11]	7.5	−49.16	0.4; 2.4	10	Skin cube
[13]	2.5	N/A	2.4	25	Skin cube
This paper	5.35	−33.65	0.4; 0.9	10–16	Three-layer model

Fig. 3. Reflection coefficient of the antenna ((a) at 400 MHz and (b) at 915 MHz).

Table 3. Dielectric constants of human tissue [14]

Frequency		Bone	Muscle	Skin
403 MHz	ε_r	13.22	57.15	46.81
	σ (S/m)	0.09	0.79	0.69
915 MHz	ε_r	12.45	54.98	41.35
	σ (S/m)	0.15	0.93	0.85

Fig. 4. 2D radiation pattern of the antenna at 10 and 16 mm implantation depth ((a) at 403 MHz and (b) at 915 MHz).

extracted from the CST database. All the numerical results are obtained with CST Studios [14] software.

As seen in Fig. 3, the designed antenna is not sensitive to the implantation depth. The −10 dB bandwidth at 403 and 915 MHz are 80 and 60 MHz, which covers the entire corresponding authorized band.

Radiation pattern and efficiency

The radiation pattern is calculated in the center of the frequency band: 403 and 915 MHz. The 2D radiation patterns are presented in Fig. 4.

The antenna is implanted at 10 mm depth. At MedRadio band (403 MHz), the maximum gain in far field is around −33.5 dB and toward the Z axis (see Fig. 2 for axis positioning). At ISM band (915 MHz), the gain is −33.65 dB. It is worth pointing out that the antenna has a better maximum gain at deeper location: at 16 mm depth, its gain increases to −31.6 dB at 403 MHz and −33.1 dB at 915 MHz since the radiation pattern has a narrower main lobe.

A comparison of gain is also presented in Table 2. In [7], the designed antenna has a gain of −15 dB when implanted into a muscle cylinder with a tissue-mimicking phantom. But the antenna is embedded only 3 mm deep which is not as realistic
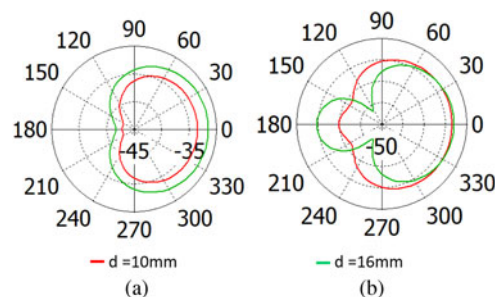
as in this paper because the implantation at this depth is more vulnerable and more difficult to realize. In [9], the antenna has a similar size to the one in this paper; the gain at 915 MHz is −33.41 dB when implanted into an anatomical head tissue. But this study is for more specific uses and less useful for other general implantation cases. The implantation depth is 10 mm which is less deep and the antenna is slightly larger compared with the antenna in this paper. In [11], the antenna has a gain of −49.16 dB at 403 MHz when implanted 10 mm into a skin box which is lower than the one here.

Specific absorption rate (SAR)

SAR is a vital parameter that indicates the safety level of an embedded antenna; it represents the average amount of electromagnetic power that can be absorbed by human body. The two IEEE standards about SAR limits [15, 16] point out that the value of SAR for every 1 or 10 g of human tissue cannot be higher than 1.6 and 2 W/kg, respectively. In Table 4, the maximum input power for the antenna that satisfies each SAR limit at 403 and 915 MHz for implantation depths of 10 or 16 mm is given.

Table 4. Maximum input power for the antenna

Max input power (mW)	1 g-average		10 g-average	
Implantation depth (mm)	10	16	10	16
403 MHz	15.38	14.99	72.22	71.17
915 MHz	14.08	14.01	86.33	91.19
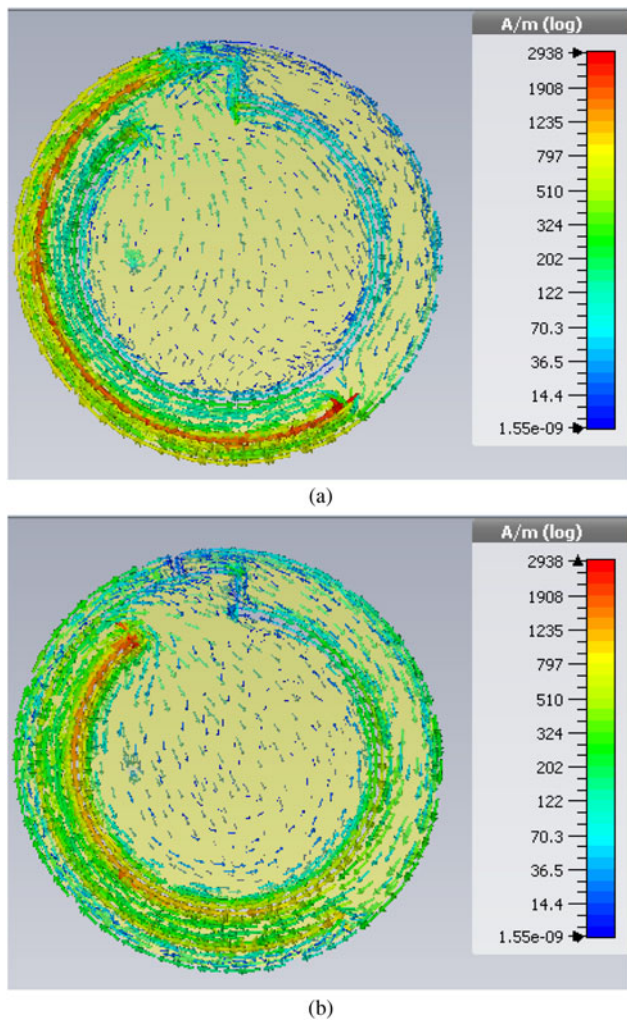
Fig. 5. Surface current on the radiating patch at around phase = 250° ((a) at 402 MHz and (b) at 915 MHz).

Surface current

The surface current is also an important factor, especially during the antenna's design. It shows the polarization of the antenna and the current path on the patch. This helps adjust the antenna in order to resonate in the correct frequency range. Figure 5 shows the surface current on the radiating patch at 402 and 915 MHz.

As seen, the current along the external slot reaches its peak value when the antenna resonates at 402 MHz and the current along the internal slot reaches its peak at 915 MHz. This shows the radiation and the polarization mode of the antenna.

In-body/off-body interaction

The antenna is designed to receive energy and emit signal for information exchange at the same time, therefore it is necessary to evaluate its capacity and efficiency with a more realistic situation in order to examine its performance and also to choose the best energy transmitting frequency band. In this section, a half-wavelength (in air) dipole is used as an external device for both energy and information transfer at the operating frequencies as shown in Fig. 2.

The external device is located face-to-face with the main lobe of the antenna at its operating frequency.

As a reception device from transmission dipole

The value of power received is a significant parameter to evaluate the performance of the implantable device as a reception device. In Table 5, the power received by the embedded antenna from the external dipole as well as the implantation depth and the dipole to skin distance in each case is provided. It should be noted that for each frequency band, there exist different radiated power limits: −16 dBm (25 µW) at MedRadio band (401–406 MHz) [17] and 30 dBm (1 W) at ISM band (902–928 MHz) [18].

With the maximum authorized input power, the antenna is able to receive 4000 times more energy (nearly 1000 times when embedded deeper) in the ISM band than in the MedRadio band. Therefore, in our case, the ISM band (902–928 MHz) is chosen as the energy transmission band. The SAR values in both cases are much lower than the limits.

As an emission device to reception dipole

It is also necessary to analyze the power redelivered to the external dipole to ensure the possibility to receive signal from the circular antenna when it is embedded inside human body.

In [19], an RF-DC conversion circuit is proposed with an efficiency of 33.1%. If 5% of total converted DC power is assumed to be used for emitting signal, for each distance between the energy delivery dipole and the skin surface, there is always a corresponding maximum distance between the reception dipole and the skin surface in order to ensure the connection (energy received by the reception dipole ≥−90 dBm [20] which is the minimum power that can be received by mobile phones without information loss) for every different implantation depth. The results are presented in Table 6. For example, if a dipole at 915 MHz is fed with 30 dBm and is 375 mm from the tissue surface while the implanted antenna is at 16 mm depth, then under the above restrictions an external dipole (at MedRadio band) should be placed at a maximum distance of 155 mm.

Furthermore, in [21] a table of sensors is presented together with their average power consumption. This also validates the usefulness of the antenna in this paper.

Table 5. Results as reception device

	Embedded depth (mm)	External dipole–arm surface distance (mm)	Max authorized emission power (dBm)	Max power received (dBm)	SAR (W/kg)	
					1 g-average	10 g-average
403 MHz	10	105	−16	−54.5	1×10^{-4}	3×10^{-5}
	10	375	−16	−66.2	2×10^{-6}	1×10^{-6}
	16	375	−16	−64.5	2×10^{-6}	1×10^{-6}
915 MHz	10	105	30	−18.5	0.32	0.22
	10	375	30	−28.76	0.024	0.017
	16	375	30	−31.35	0.025	0.018

Table 6. Results as emission device

Implantation depth (mm)	Distance between energy delivery dipole and arm surface at 915 MHz (mm)	Maximum distance between reception dipole and arm surface at 400 MHz (mm)
10	105	450
	375	185
	700	105
16	105	425
	375	155
	625	105

Table 7. Comparison of dielectric characteristics

	Ground pork	Human muscle
ε_r	39.8	54.9
σ (S/m)	0.65	0.93

Table 8. Parameters of the newly designed antenna

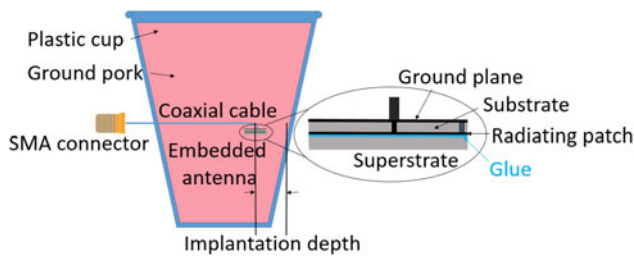| Parameter	Value (mm)	Parameter	Value (deg)
R_1	4.82	θ_1	22
R_2	3.68	θ_2	18
w_1	0.15	θ_3	141
w_2	0.32	θ_4	179
t_1	0.64		
D_{patch}	10.8		
D_{ground}	11		

Fig. 6. Simulation model for predicting changes during measurements.

Experimental measurements

Electromagnetic simulation of the experimental case

During the experiment, ground pork meat is used as replacement for "human tissue" since it is more realistic than using liquid material to emulate dielectric properties of human tissue for various RF frequencies [22]. A cylindrical plastic cup is used to guarantee the cylindrical form to simulate the human arm. Due to the absence of the bone and change in the shape of the tissue, a further simulation with these experimental materials is realized in order to match the situation. The simulation structure is shown in Fig. 6.

The antenna is embedded with the coaxial cable in a cup of ground pork. The thickness of the plastic cup is 0.5 mm and the implantation depth is calculated from the center of the antenna to the inner surface of the plastic cup at the same height level.

It is worth pointing out that although in Fig. 6 the antenna is embedded together with the coaxial cable, in the real case, the coaxial cable is no longer used because the antenna will serve as a power receiving device. It will be directly connected with a rectifying circuit and then feed the corresponding sensor.

Although porcine meat has been used frequently as a replacement of human tissue thanks to its easy accessibility and its similarity of dielectric properties and biological responses to human tissues [23], there are still slight differences between the electrical properties of the two tissues, especially when it is adipose tissue. Table 7 shows the electrical characteristics of ground meat and human muscle at 915 MHz [22, 24].

Due to this change of environmental characteristics, some fine-tuning should be done to the antenna design in order to obtain the same resonant frequencies as in the simulations. Table 8 shows the parameters of the newly designed and fabricated antenna.

In the new design, the two resonant frequencies are moved slightly to lower frequencies (by reducing the radius of the two slots respectively) in order to leave a margin for the frequency shifting caused by a decrease in the dielectric constant. Furthermore, a glue layer of 0.8 mm ($\varepsilon_r \approx 3.5$) to stick the substrate together with the superstrate is also taken into account. The metallic patch has a diameter of 10.8 mm but the diameters of substrate, superstrate, and ground plane are all increased to 11 mm, in order to cover the patch. This new design avoids the direct contact between the patch and the surrounding tissue and thus becomes more robust to the environmental change and has a higher gain.
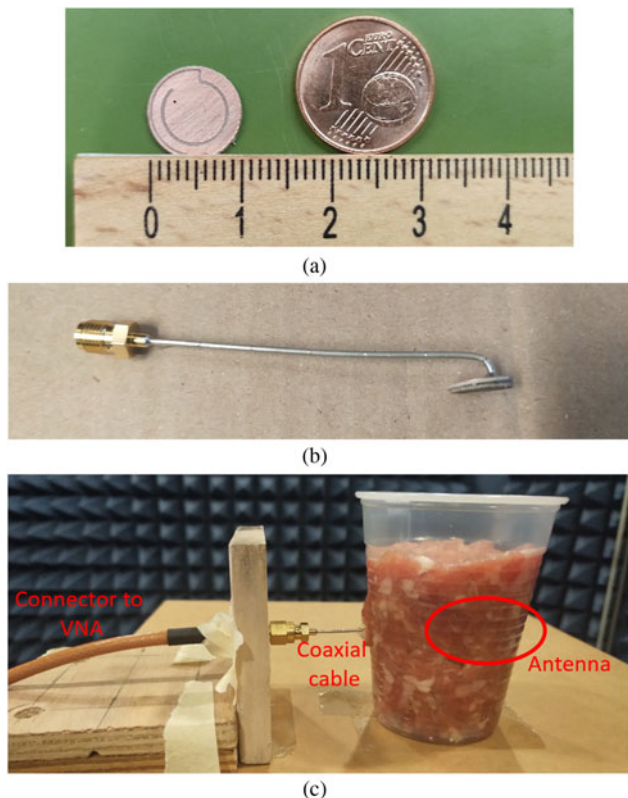
Fig. 7. (a) Fabricated antenna compared with one euro cent. (b) Complete antenna with a coaxial cable and superstrate. (c) Antenna embedded into minced pork.

This impedance of the antenna is standardized to $110\,\Omega$ in order to obtain a good performance.

Measurement results

The measurements are performed in an anechoic chamber. Figure 7(a) shows the fabricated antenna in comparison with a euro cent. Figure 7(b) shows the antenna with glued superstrate and soldered together with the coaxial cable. Figure 7(c) shows the structure under measurement inside the anechoic chamber. The whole antenna is embedded in the ground pork with a certain implantation depth measured from the outside. Then the connector is fixed onto the measurement platform in order to avoid uncertainties.

The coaxial cable is folded behind the main radiating direction in order to minimize the influence of radiation that comes from the cable. Moreover, the glue that surrounds the radiating patch may also lead to the isolation of the antenna from the pork tissue. The scenario is presented in Fig. 8(a).

Figure 8(b) shows the measured results of the reflection coefficient obtained by the Vector Network Analyzer Agilent E8363b as compared with the corresponding simulated S_{11}. The results at the first resonant frequency of 403 MHz are in satisfactory agreement. For the second resonant frequency, there is a shift in the resonance of around 25 MHz. This is because, on the one hand, the dielectric constant of the pork tissue is lower than that of the human muscle; on the other hand, the air bubbles that exist among the ground pork meat may also decrease the equivalent permittivity of the surrounding environment. Therefore, the antenna resonates at a higher frequency than designed. However, in general the measurement results and simulation results match well with each other.
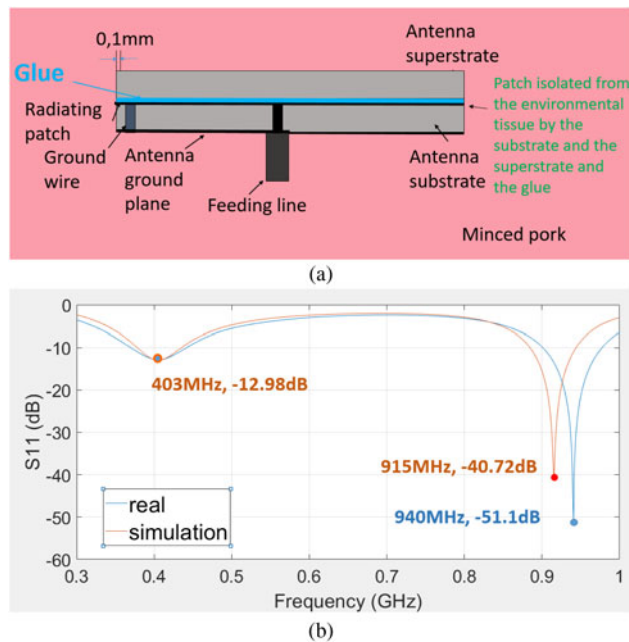

Fig. 8. (a) Experimental structure of the fabricated antenna. (b) Measurement results compared with simulation results.
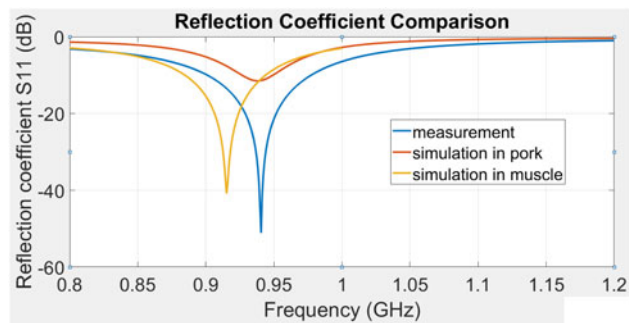

Fig. 9. Comparison of different reflection coefficient results.

In order to validate this assumption, a new simulation using the dielectric properties of pork is performed and the reflection coefficient S_{11} at 915 MHz band is compared with the experimental result. This is shown in Fig. 9.

As shown in Fig. 9, the result of the simulated S_{11} in pork is much closer to the measurement result compared with the simulation in muscle, which validates the previous assumption that this shifting is caused by the difference between the pork and human tissue.

Conclusion

In this paper, a miniaturized circular antenna is designed for deep-body wireless biomedical applications. The antenna is studied while embedded into a three-layer cylindrical model of arm and its performance is evaluated. The dual resonant frequency covers MedRadio (401–406 MHz) and ISM bands (902–928 MHz). The antenna has a gain of −31.6 dB at 403 MHz and −33.1 dB at 915 MHz, respectively. The in-body/off-body link is also analyzed. First, we assess the amount of power that could be received from an external dipole at the maximum authorized input power in order to select the appropriate energy

transmission band. Then the amount of power that could be redelivered to the external device is also calculated, and the distance limits to ensure reliable connection are shown in the paper. Finally, the antenna is fabricated and tested in an anechoic chamber. Although slight differences are observed between the measurement and simulation results, the deviation is acceptable while the source of discrepancies (air bubbles and change in the dielectric properties of tissue) is identified.

In the future, several transmission and link budget scenarios will be tested and measured in the anechoic chamber. The newly design antenna will also be tested.

Supplementary material. The supplementary material for this article can be found at https://doi.org/10.1017/S1759078720000197.

References

1. **ITU-R (International Telecommunications Union-Radiocommunications),** Radio regulations, section 5.138 and 5.150, ITU. Geneva, Switzerland, [Online].
2. **Bakogianni S and Koulouridis S** (2016) An implantable planar dipole antenna for wireless MedRadio-band biotelemetry devices. *IEEE Antennas and Wireless Propagation Letters* **15**, 234–237.
3. **FCC**. Washington, D.C., USA, Federal Communications Commission 2012. [Online]. Available at http://www.fcc.gov.
4. **Chirwa LC, Hammond PA, Roy S and Cumming DRS** (2003) Electromagnetic radiation from ingested sources in the human intestine between 150 MHz and 1.2 GHz. *IEEE Transactions on Biomedical Engineering* **50**, 484–492.
5. **Kim J and Rahmat-Samii Y** (2004) Implanted antennas inside a human body: simulations, designs, and characterizations. *IEEE Transactions on Microwave Theory and Techniques* **52**, 1934–1943.
6. **Luu QT, Koulouridis S, Diet A, Le Bihan Y and Pichon L** (2017) Investigation of inductive and radiating energy harvesting for an implanted biotelemetry antenna. 2017 *11th European Conference on Antennas and Propagation, EUCAP* 2017, pp. 160–163.
7. **Ali MM, Bashar MEI and Hosain MK** (2017) Circular planner inverted-F antenna for implantable biomedical applications. 2017 *2nd International Conference on Electrical & Electronic Engineering* (ICEEE), 1, pp. 1–4.
8. **Liu C, Guo YX and Xiao S** (2012) Compact dual-band antenna for implantable devices. *IEEE Antennas and Wireless Propagation Letters* **11**, 1508–1511.
9. **Kiourti A and Nikita KS** (2012) Miniature scalp-implantable antennas for telemetry in the MICS and ISM bands: design, safety considerations and link budget analysis. *IEEE Transactions on Antennas and Propagation* **60**, 3568–3575.
10. **Karacolak T, Cooper R and Topsakal E** (2009) Electrical properties of rat skin and design of implantable antennas for medical wireless telemetry. *IEEE Transactions on Antennas and Propagation* **57**, 2806–2812.
11. **Mohamed AE and Sharawi MS** (2017) Miniaturized dual-wideband circular patch antenna for biomedical telemetry. 2017 *11th European Conference on Antennas and Propagation* (EUCAP), pp. 1027–1030.
12. **Ding S, Koulouridis S and Pichon L** (2019) A dual-band miniaturized circular antenna for deep in body biomedical wireless applications. *2019 13th European Conference on Antennas and Propagation (EuCAP)*, Krakow, Poland, pp. 1–4.
13 **Shubair RM, Salah A and Abbas AK** (2015) Novel implantable miniaturized circular microstrip antenna for biomedical telemetry. IEEE Antennas and Propagation Society, AP-S International Symposium (Digest), 2015 October, pp. 947–948.
14. **Computer Simulation Technology (CST) STUDIO SUITE**. Ver 2017, CST AG, Germany.
15. **IEEE** (1999) IEEE standard for safety levels with respect to human exposure to radiofrequency electromagnetic fields, 3 kHz to 300 GHz, IEEE Standard C95.1.
16. **IEEE** (2005) IEEE standard for safety levels with respect to human exposure to radiofrequency electromagnetic fields, 3 kHz to 300 GHz, IEEE Standard C95.1.
17. **International Telecommunications Union** (1998) Recommendation ITU-R RS.1346.
18. **FCC**. 15.209, Standard Specification for Radiated emission limits, general requirements.
19. **Bakogianni S and Koulouridis S** (2016) Design of a novel miniature implantable rectenna for in-body medical devices power support. 2016 *10th European Conference on Antennas and Propagation* (EUCAP).
20. **Sauter M** (2010) *From GSM to LTE. An Introduction to Mobile Networks and Mobile Broadband*. Cologne, Germany: Wiley, 2014, p. 251.
21. **Ding S, Koulouridis S and Pichon L**. (2019) Miniaturized implantable power transmission system for biomedical wireless applications. *Wireless Power Transfer*, pp. 1–9.
22. **Gabriel S, Lau R and Gabriel C** (1996) The dielectric properties of biological tissues: II. Measurements on the frequency range 10 Hz to 20 GHz. *Physics in Medicine and Biology* **41**, 2251–2269.
23. **Vallejo M, Recas J, del Valle PG and Ayala JL** (2013) Accurate human tissue characterization for energy-efficient wireless on-body communications. *Sensors* **13**, 7546–7569.
24. **Deneris ZA, Pe'a DE and Furse CM** (2019) A layered pork model for subdermal antenna tests at 433 MHz. *IEEE Journal of Electromagnetics, RF and Microwaves in Medicine and Biology* **3**, 171–176.

Shuoliang Ding was born in Shenyang, China in 1994. He received his diploma engineer degree from the Ecole Centrale de Nantes in France and a diploma master degree from Beihang University in Beijing, China in 2017. He is currently pursuing his Ph.D. degree in CentraleSupelec in Paris, France. In 2017, he joined the Group of Electrical Engineering in Paris (GeePs). During his Ph.D. study, he has authored several papers in international conferences. His current research interests include bio-electromagnetics, antenna theory, implantable antenna design, and wireless powering devices for biomedical applications.

Stavros Koulouridis was born in 1975, in Athens, Greece. He received his Diploma Engineer degree in electrical and computer engineering and his Ph.D. degree in microwave engineering from the National Technical University of Athens, Greece, in 1999 and 2003, respectively. From 1999 to 2003 he worked as a Research Engineer in Microwave and Fiber Optics Lab and Biomedical Simulations and Imaging Unit, National Technical University of Athens. He taught several classes in the School of Pedagogic and Technological Education (ASPAITE) from 2000 to 2003. He was also a teaching assistant from 2000 to 2002 at the National Technical University of Athens. From 2004 to 2008, he worked as Postdoctoral Researcher at the Electroscience Laboratory, The Ohio State University, Columbus, OH, USA. In March 2009, he joined Electrical and Computer Engineering Department, University of Patras, Greece and since August 2013, he holds an Assistant Professor position. From 2015 to 2016, he was visiting professor in the Group of Electrical Engineering – Paris (GeePs)/CNRS-CentraleSupelec – Univ. Paris-Sud – Université Paris-Saclay – Sorbonne Université. He leads the Microwave Communications group. His research interests include antenna and microwave devices design, development and fabrication of novel materials, microwave applications in medicine, electromagnetic optimization techniques, and applied computational electromagnetics. He was the recipient of a 3 year Ph.D. Scholarship on Biomedical Engineering from Hellenic State Scholarships Foundation in 2001. In May 2005, he received the annual award for the best dissertation from the National Technical University of Athens. He is the Chair of IEEE AP/MTT/ED Local Greek Chapter. He was the General Chair of IWAT 2017 (International Workshop in Antennas Technology). He has published over

80 refereed journals and conference proceeding papers. He is serving as reviewer for several scientific international journals.

Lionel Pichon received his Dip. Eng. from Ecole Supérieure d'Ingénieurs en Electronique et Electrotechnique in 1984. In 1985, he joined the Laboratoire de Génie Electrique de Paris where he earned a Ph.D. in electrical engineering in 1989. He got a position at the CNRS (Centre National de la Recherche Scientifique) in 1989. He is now Directeur de Recherche (Senior Research Scientist) in GeePs (Group of electrical engineering – Paris), a laboratory belonging to four institutions: CNRS, CentraleSupélec, Université Paris-Saclay, and Sorbonne Université. His research interests include computational electromagnetics for wave propagation, scattering, and electromagnetic compatibility.